# Myocardial fibrosis in the right ventricle detected on ECG gated 320 slice CT showed a short term poor prognosis in subjects with pulmonary hypertension

Koya Ozawa [a], Nobusada Funabashi [a,*], Akihisa Kataoka [a], Nobuhiro Tanabe [b], Noriyuki Yanagawa [b], Koichiro Tatsumi [b], Yoshio Kobayashi [a]

[a] Department of Cardiovascular Medicine, Chiba University Graduate School of Medicine, 1-8-1 Inohana, Chuo-ku, Chiba City, Chiba 260-8670, Japan
[b] Department of Respirology, Chiba University Graduate School of Medicine, 1-8-1 Inohana, Chuo-ku, Chiba City, Chiba 260-8670, Japan

ARTICLE INFO

*Article history:*
Received 21 November 2012
Accepted 18 January 2013
Available online 28 March 2013

*Keywords:*
Myocardial fibrosis
Right ventricle
ECG gated 320 slice CT
Short term poor prognosis
Pulmonary hypertension

Presence of myocardial fibrosis in the right ventricular (RV) myocardium (RVM) may contribute to a poor prognosis in a subject with Tetralogy of Fallot [1]. If myocardial fibrosis in RVM can be detected in subjects who have other diseases with increased RV pressure, such as pulmonary arterial hypertension (PAH) or chronic thromboembolic pulmonary hypertension (PH) (CTEPH), a prognosis may be predicted.

Magnetic resonance imaging (MRI) can detect myocardial fibrosis in the left ventricular (LV) myocardium (LVM) [2], but some subjects with PAH or CTEPH cannot tolerate long acquisition time in the narrow space of an MRI scanner.

Recently, enhanced multislice computed tomography (CT), as well as MRI, was shown to detect myocardial fibrosis in LVM as contrast defect in the early phase and abnormal enhancement in the late phase [3].

In subjects with PAH and CTEPH, evaluation of the presence of thrombi in the pulmonary artery (PA) using CT is essential. Furthermore, quantitative evaluation of RV function by retrospective electrocardiogram (ECG) gating CT is determined as appropriate in the ACCF/SCCT/ACR/AHA/ASE/ASNC/NASCI/SCAI/SCMR 2010 appropriate use criteria for cardiac CT [4]. Since subjects with PAH and CTEPH show hypertrophied RVM, by adding late acquisition with prospective ECG gating CT, myocardial fibrosis can be visualized easily with minimum radiation exposure addition.

To evaluate the significance of presence of myocardial fibrosis in RVM on CT, as represented as an early defect in the early phase and conversely abnormal enhancement in the late phase on enhance CT, in PH subjects who underwent ECG gated enhanced 320 slice CT.

A total of 56 PH subjects confirmed on right heart catheterization (RHC) (15 males, age 57 ± 15 years, 33 CTEPH, 21 PAH, and 2 others) underwent ECG gated 320 slice CT (Aquilion one, Toshiba Medical) to evaluate PA, and transthoracic echocardiogram (TTE) within 3 months without any clinical incidents. Subjects were followed for a median of 9.5 months and all cause death was evaluated.

Two dimensional TTE was performed to evaluate RV and right atrial (RA) sizes, as well as RV systolic and diastolic functions. The parameters included a measure of tricuspid annular plane systolic excursion (TAPSE), estimated systolic PA pressure (sPAP), acceleration time per ejection time (AcT/ET), tricuspid valve (TV) systolic velocity (TV S′) and TV early diastolic tricuspid inflow velocity (E)/early diastolic tricuspid annulus velocity (E′) (TV E/E′), and cardiac output (CO).

To obtain not only images of the whole heart including RV and coronary arteries, but also images of the PA, all CT scans were obtained using a double volume conventional scan with retrospective ECG-gating using 320-slice CT with a 0.5 mm slice thickness and 0.35 s/rotation with a downward direction. Tube voltage was set at 120 kV and tube current was set at 580 mA with tube current dose modulation. We injected 60 ml of contrast material (350 mg I/ml) at 3.5 ml/s, followed by injection of a saline-to-contrast material mixture (40 ml contrast material at 2.0 ml/s and 30 ml saline at 1.5 ml/s), followed by injection of 20 ml pure saline at 1.5 ml/s [5,6]. All CT examinations were performed for a normal workup to diagnose or evaluate PH, with a scanning delay of 20–30 s for optimal PA visualization. Single volume conventional scan with prospective ECG-gating was added and if there was abnormal enhancement in RVM, we regarded this as myocardial fibrosis (Fig. 1).

All RHCs were performed by pneumologists with more than 5 years experience in managing PH patients. A Swan–Ganz thermodilution catheter was used and a jugular approach was preferred. sPAP, diastolic (dPAP) and mean PA (mPAP) pressures, RA pressure, CO and cardiac index (CI) were measured by thermodilution method and pulmonary vascular resistance.

Myocardial fibrosis in RVM was detected in 16 subjects (5 males, 56 ± 12 years old, 9 CTEPH, 6 PAH and 1 other). There were no significant differences of frequency of myocardial fibrosis in RVM among the three groups (Fig. 2).

Comparing subjects with and without myocardial fibrosis in RVM on CT (Tables 1–5), only CO (l/min) calculated on TTE was significantly lower, and the occurrence of all cause death during the observation period was significantly higher in subjects with myocardial fibrosis in RVM than in subjects without myocardial fibrosis in RVM (both $P<0.05$), even though there were no significant differences between the two groups in other factors, especially hemodynamic state parameters on TTE (Table 2), CT (Table 3), and RHC (Table 4). Furthermore the occurrence of all cause death was significantly higher in subjects with myocardial fibrosis in RVM than in subjects without myocardial fibrosis in RVM on CT ($P<0.05$) (Table 5).

Significant differences between subjects with and without myocardial fibrosis in RVM were observed at each time point when the whole follow-up period was compared by further Kaplan–Meier analysis and log rank test ($P=0.024$) (Fig. 3).

The presence of myocardial fibrosis in RVM detected on ECG-gated 320 slice CT may influence the short term poor prognosis in PH subjects, even though there were no significant differences in hemodynamic state parameters acquired from CT, TTE and RHC (except CO on TTE) between subjects with and without myocardial fibrosis in RVM on CT.

In contrast to hemodynamic state parameters, which tend to fluctuate, the presence of myocardial fibrosis in RVM is a permanent, irreversible, and organized morphological parameter that may be useful for accurately predicting the prognosis of PH subjects.

To our knowledge, our study is the first to describe the evaluation of myocardial fibrosis in RVM based on CT heart images in PH subjects.

Since the gold standard for the detection of myocardial fibrosis is MRI [2], the detection of myocardial fibrosis on CT should be compared with that detected on MRI, both qualitatively and quantitatively, to evaluate the efficiency of CT for such detection, even though subjects with PAH or CTEPH may not tolerate long acquisition time in the narrow space of an MRI scanner.

* Corresponding author. Tel.: +81 43 222 7171x5264.
*E-mail address:* nobusada@w8.dion.ne.jp (N. Funabashi).

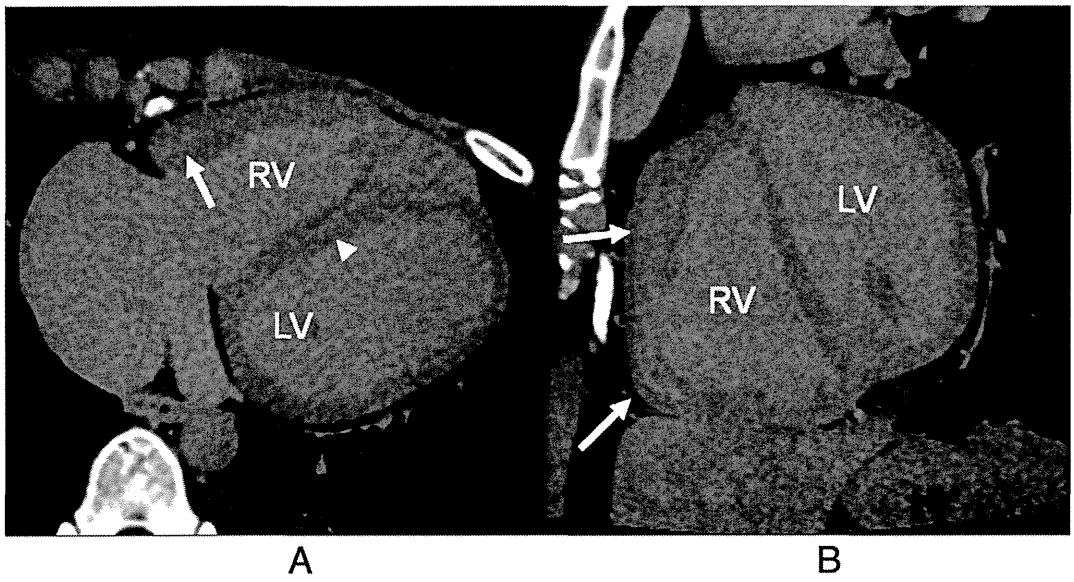


**Fig. 1.** Typical imaging of myocardial fibrosis (arrows and arrow head in right ventricular (RV) myocardium) in the late phase acquisition.A: Axial source image.B: Multiplanar reconstruction image of short axis of RV.Compared with the left ventricular (LV) myocardium, hypertrophied RV myocardium showed higher computed tomography attenuation in RV anterior to inferior wall (arrows) and RV sided inter ventricular septum (arrowhead).

Our study population was small (N=56), retrospective and non-randomized and located in a single center. The follow-up time was short (median of 9.5 months). Further prospective and long term studies are desired in a larger population. Compared with a non-ECG gated helical scan, the combination of double volume conventional scan with retrospective ECG gated in early phase and single volume conventional scan with prospective ECG gating requires a greater radiation dose, even though information of RV function and coronary arteries can be obtained.

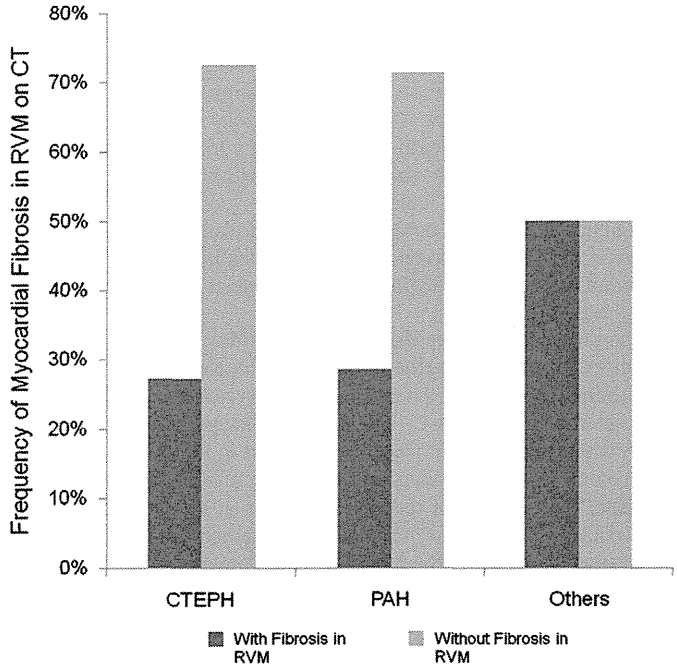


**Fig. 2.** Frequency of myocardial fibrosis in the right ventricular myocardium (RVM) on computed tomography (CT) in each group.There were no significant differences of frequency of fibrosis in RVM among the three groups: chronic thromboembolic pulmonary hypertension (CTEPH) (N=33), pulmonary arterial hypertension (PAH) (N=21), and others (N=2) (Chi square test P=0.788).

**Table 1**
Comparison of patient characteristics and general hemodynamic state parameters between subjects with and without myocardial fibrosis in the right ventricular myocardium (RVM) on computed tomography.
There were no significant differences in all these parameters between the two groups.

| | With myocardial fibrosis in RVM N=16 | Without myocardial fibrosis in RVM N=40 | P value |
|---|---|---|---|
| Age (years) | 56±12 | 57±16 | 0.788 |
| Females (%) | 11 (61.8%) | 30 (75.0%) | 0.633 |
| Systolic blood pressure (mm Hg) | 116±18 | 115±17 | 0.786 |
| Diastolic blood pressure (mm Hg) | 74±15 | 70±11 | 0.190 |
| Brain natriuretic peptide (pg/ml) | 179±252 | 181±293 | 0.987 |
| Six minute walk test (m) | 387±110 | 370±94 | 0.582 |

**Table 2**
Comparison of transthoracic echocardiogram (TTE) findings between subjects with and without myocardial fibrosis in the right ventricular (RV) myocardium (RVM) on computed tomography.
Only cardiac output was significantly lower in subjects with myocardial fibrosis in RVM than in subjects without myocardial fibrosis in RVM (P<0.05).
PASP, TAPSE, AcT/ET, TV S′ and TV E/E′ indicate pulmonary arterial systolic pressure, tricuspid annular plane systolic excursion, acceleration time per ejection time, tricuspid valve (TV) systolic velocity (S′) and TV early diastolic tricuspid inflow velocity (E)/early diastolic tricuspid annulus velocity (E′), respectively.

| TTE findings | With myocardial fibrosis in RVM N=16 | Without myocardial fibrosis in RVM N=40 | P value |
|---|---|---|---|
| RV end diastolic diameter (mm) | 40.5±6.7 | 43.0±8.6 | 0.417 |
| RV end systolic diameter (mm) | 32.6±9.3 | 34.5±1.7 | 0.565 |
| Estimated PASP (mmHg) | 74±23 | 68±24 | 0.419 |
| TAPSE (mm) | 20±6 | 17±6 | 0.206 |
| RV outflow AcT/ET | 0.26±0.06 | 0.27±0.08 | 0.654 |
| Cardiac output (l/min) | 3.5±1.0 | 4.4±1.1 | 0.011* |
| TV S′ | 9.6±1.9 | 11.9±2.5 | 0.108 |
| TV E/E′ | 6.4±2.3 | 6.0±3.9 | 0.785 |

* P<0.05.

**Table 3**
Comparison of electrocardiogram (ECG) gated computed tomography (CT) findings between subjects with and without myocardial fibrosis in the right ventricular (RV) myocardium (RVM) on CT.
There were no significant differences in all these parameters between the two groups. RA indicates right atria.

| ECG gated CT findings | With myocardial fibrosis in RVM N = 16 | Without myocardial fibrosis in RVM N = 40 | P value |
|---|---|---|---|
| RV wall thickness (diastolic) (mm) | 3.8 ± 1.2 | 3.3 ± 1.1 | 0.165 |
| RV wall thickness (systolic) (mm) | 5.5 ± 1.9 | 5.1 ± 1.7 | 0.493 |
| RV end diastolic volume (ml) | 156 ± 75 | 138 ± 75 | 0.438 |
| RV end systolic volume (ml) | 106 ± 60 | 96 ± 70 | 0.238 |
| RV ejection fraction (%) | 34.6 ± 13 | 34.6 ± 14 | 0.992 |
| RA end diastolic volume (ml) | 121 ± 68 | 116 ± 61 | 0.768 |
| RA end systolic volume (ml) | 95 ± 61 | 93 ± 60 | 0.914 |

**Table 4**
Comparison of right heart catheter (RHC) findings between subjects with and without myocardial fibrosis in the right ventricular myocardium (RVM) on computed tomography (CT).
There were no significant differences in all these parameters between the two groups. sPAP, dPAP, mPAP and PVR indicate systolic pulmonary arterial pressure (PAP), diastolic PAP, mean PAP, and pulmonary vascular resistance, respectively.

| RHC findings | With myocardial fibrosis in RVM N = 16 | Without myocardial fibrosis in RVM N = 40 | P value |
|---|---|---|---|
| sPAP (mm Hg) | 78 ± 16 | 74 ± 27 | 0.571 |
| dPAP (mm Hg) | 26 ± 9 | 25 ± 10 | 0.744 |
| mPAP (mm Hg) | 46 ± 10 | 43 ± 16 | 0.497 |
| Pulmonary capillary wedge pressure (mm Hg) | 8.8 ± 3.4 | 8.5 ± 3.8 | 0.779 |
| Cardiac output (l/min) | 4.3 ± 1.2 | 4.5 ± 1.0 | 0.539 |
| Cardiac index (l/min/m$^2$) | 2.9 ± 0.9 | 2.8 ± 0.6 | 0.629 |
| PVR (dyne · s · cm$^{-5}$) | 733 ± 84 | 701 ± 58 | 0.759 |

Detection of myocardial fibrosis in RVM on CT was very subjective and strict differentiation of myocardial fibrosis with myocardial edema due to inflammation cannot be achieved (additional performance of 18F-FDG-PET may be desired) [7,8].

Myocardial fibrosis in RVM as detected on ECG gated 320 slice CT in PH subjects is a permanent, irreversible, and organized morphological parameter that may be useful for accurately predicting the prognosis of PH subjects.

This work is partially supported by a Grant from Japan Heart Foundation Young Investigator's Research Grant. The authors of this manuscript have certified that they comply with the Principles of Ethical Publishing in the International Journal of Cardiology.

## References

[1] Babu-Narayan SV, Kilner PJ, Li W, et al. Ventricular fibrosis suggested by cardiovascular magnetic resonance in adults with repaired Tetralogy of Fallot and its relationship to adverse markers of clinical outcome. Circulation 2006;113:405–13.
[2] Moon JC, Reed E, Sheppard MN, et al. The histologic basis of late gadolinium enhancement cardiovascular magnetic resonance in hypertrophic cardiomyopathy. J Am Coll Cardiol 2004;43:2260–4.
[3] Nieman K, Shapiro MD, Ferencik M, et al. Reperfused myocardial infarction: contrast-enhanced 64-section CT in comparison to MR imaging. Radiology 2008;247:49–56.


http://dx.doi.org/10.1016/j.ijcard.2013.01.251

**Table 5**
Comparison of occurrence of events during observation periods between subjects with and without myocardial fibrosis in the right ventricular myocardium (RVM) on computed tomography (CT).
The occurrence of all cause death was significantly higher in subjects with myocardial fibrosis in RVM than subjects without myocardial fibrosis in RVM (P<0.05).

| | With myocardial fibrosis in RVM N = 16 | Without myocardial fibrosis in RVM N = 40 | P value |
|---|---|---|---|
| Event | 5 (31.3%) | 4 (10.0%) | 0.05 |
| Congestive heart failure | 1 | 4 | 0.657 |
| Stroke | 2 | 0 | 0.023 |
| Nonfatal myocardial infraction | 0 | 0 | – |
| All cause death | 2 (12.5%) | 0 (0%) | 0.023* |

* P<0.05.

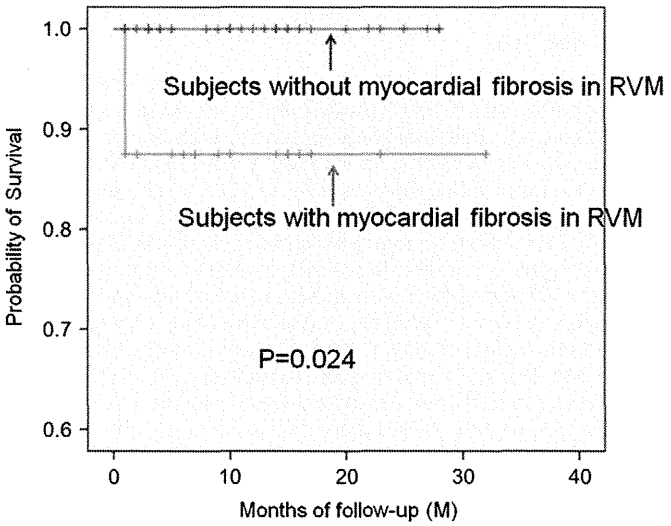


**Fig. 3.** Kaplan–Meier survival curves for occurrence of all cause death.All cause death was observed more frequently in patients with myocardial fibrosis in the right ventricular myocardium (RVM) on computed tomography (CT) than in those without myocardial fibrosis in RVM on CT (log-rank test, P = 0.024) during the observation period.

[4] Taylor AJ, Cerqueira M, Hodgson JM, et al. ACCF/SCCT/ACR/AHA/ASE/ASNC/NASCI/SCAI/SCMR 2010 appropriate use criteria for cardiac computed tomography. A report of the American College of Cardiology Foundation Appropriate Use Criteria Task Force, the Society of Cardiovascular Computed Tomography, the American College of Radiology, the American Heart Association, the American Society of Echocardiography, the American Society of Nuclear Cardiology, the North American Society for Cardiovascular Imaging, the Society for Cardiovascular Angiography and Interventions, and the Society for Cardiovascular Magnetic Resonance. J Am Coll Cardiol 2010;56:1864–94.
[5] Uehara M, Funabashi N, Ueda M, et al. Quality of coronary arterial 320-slice computed tomography images in subjects with chronic atrial fibrillation compared with normal sinus rhythm. Int J Cardiol 2011;150:65–70.
[6] Uehara M, Funabashi N, Takaoka H, Komuro I. Quality of coronary arterial 320-slice computed tomography images compared with 16-slice computed tomography images in subjects with chronic atrial fibrillation. Int J Cardiol 2011;149:e90–3.
[7] Hama Y, Funabashi N, Ueda M, et al. Right sided heart wall thickening and delayed enhancement caused by chronic active myocarditis complicated with sustained monomorphic ventricular tachycardia. Circulation 2009;119:e200–3.
[8] Takano H, Nakagawa K, Ishio N, et al. Active myocarditis in a patient with chronic active Epstein–Barr virus infection. Int J Cardiol 2008;130:e11–3.

PLOS ONE

# The Role of Matrix Metalloproteinase in the Intimal Sarcoma-Like Cells Derived from Endarterectomized Tissues from a Chronic Thromboembolic Pulmonary Hypertension Patient

**Takayuki Jujo[1*9], Seiichiro Sakao[1 9], Masanori Tsukahara[1], Seiji Kantake[2], Miki Maruoka[3], Nobuhiro Tanabe[1], Masahisa Masuda[4], Koichiro Tatsumi[1]**

**1** Department of Respirology (B2), Graduate School of Medicine, Chiba University, Inohana Chuo-Ku, Chiba, Japan, **2** Respirology, Kimitsu Chuo Hospital, Sakurai, Kisarazu City, Japan, **3** Respirology, National Hospital Organization Chiba Medical Center, Tsubakimori, Chuo-ku, Chiba, Japan, **4** Cardiovascular Surgery, National Hospital Organization Chiba Medical Center, Tsubakimori, Chuo-ku, Chiba, Japan

## Abstract

Sarcoma-like cells (SCLs) were derived from endarterectomized tissue of a single chronic thromboembolic pulmonary hypertension (CTEPH) patient during incubation of those thrombi at second passage as described at our previous report. These cells had malignant potential, with an increased expression of matrix metalloproteinase-14 (MMP-14), leading to tumor emboli within pulmonary arteries in *in vivo* studies. The purpose of this study was to perform a more detailed evaluation of the characteristics of SCLs, and to elucidate the role of the increased expression of MMP-14 expression in the growth and death of these cells. In order to elucidate the characteristics of SCLs and to confirm the protein expression of MMP-14, three-dimentional culture, invasion assays, a Western blot analysis and immunohistochemical studies were performed. To examine the role of MMP-14 in tumorigenesis, the metalloproteinase inhibitor, batimastat, was administered to SCID mice which were subcutaneously injected with SCLs. Those mice were sacrificed on day 14 and the tumor volume was evaluated. A Western blot analysis showed the increased expression of MMP-14 in comparison to the expression in lung adenocarcinoma cells (A549). Immunohistochemistry showed that SCLs were positive for vimentin, MMP-14, MMP-2 and CD44. However, endothelial markers, such as CD31 and von Willebrand factor (vWF), were negative. The *in vivo* studies demonstrated that batimastat could suppress the growth of the subcutaneous tumors formed by the SCLs. This study suggested that MMPs had critical roles on the pathological activities of SCLs and that batimastat might have anti-proliferative and anti-invasive effects on these cells.

**Citation:** Jujo T, Sakao S, Tsukahara M, Kantake S, Maruoka M, et al. (2014) The Role of Matrix Metalloproteinase in the Intimal Sarcoma-Like Cells Derived from Endarterectomized Tissues from a Chronic Thromboembolic Pulmonary Hypertension Patient. PLoS ONE 9(1): e87489. doi:10.1371/journal.pone.0087489

**Editor:** Masataka Kuwana, Keio University School of Medicine, Japan

**Received** September 9, 2013; **Accepted** December 21, 2013; **Published** January 28, 2014



**Funding:** Takayuki Jujo was supported by The Cardiovascular Research Fund. Seiichiro Sakao was supported by Research Grants for the Respiratory Failure Research Group and the Cardiovascular Diseases (24–57) from the Ministry of Health, Labour and Welfare, Japan and the Takeda Science Foundation. The funders had no role in study design, data collection and analysis, decision to publish, or preparation of the manuscript.

**Competing Interests:** Dr. Tatsumi has received honoraria for lectures from Glaxo Smith Kline and Actelion Pharmaceutical Ltd. Dr. Tanabe has received honoraria for lectures from Actelion, Glaxo Smith Kline, Astellas and Pfizer and research grant support from Actelion Pharmaceutical Ltd. and Pfizer. The other authors report no potential conflicts of interest. This does not alter the authors' adherence to all the PLOS ONE policies on sharing data and materials.

* E-mail: naikamo_resp19184@yahoo.co.jp

9 These authors contributed equally to this work.

## Introduction

The organized thrombi of chronic thromboembolic pulmonary hypertension (CTEPH) are composed of several cell phenotypes. Some populations have high biological activities [1], and some are positive for α-smooth muscle actin (α-SMA), which were considered to be "myofibroblast-like cells" from the endarterectomized tissues of the CTEPH patient [1,2,3]. We previously showed that the myofibroblast-like cells were hyperproliferative, invasive and anchorage-independent [3], and these characteristics are considered to be cancer hallmarks [4]. We also showed that sarcoma-like cells (SCLs) derived from a single CTEPH patient could be isolated at the second passage of the myofibroblast-like cells, and these had an increased expression of matrix metalloproteinase-14 (MMP-14), and had high tumorigenic potential to form solid and undifferentiated tumors which grew along the intimal surface of the pulmonary arteries in C.B-17/lcr-scid/scidJcl mice [5]. These results suggested that the behavior of SCLs closely resembled that of pulmonary intimal sarcoma. Pulmonary intimal sarcoma is a very rare mesenchymal neoplastic tumor [6] that is highly resistant to treatments, including anti-cancer drugs.

The purpose of this study was to obtain more details about the characteristics of SCLs in comparison to A549 epithelial cancer cells, and to elucidate the role of the increased expression of MMP-14 in the growth and death of the cells. This is the further report focusing on MMP-14 following our previous report [5]. The results of this study may lead to the development of a new therapeutic approach for this uncommon sarcoma.

## Materials and Methods

### Ethic statement

All procedures performed in this study were approved by the Research Ethics Committee of Chiba University School of Medicine and Chiba University Instrumental Animal and Use Committee. Written informed consent was given by all subjects.

### Clinical presentation of the patient

SCLs were derived from a single patient. The patient was a 64 years-old man with a history of acute pulmonary embolism and consulted to a hospital because of hemoptysis, which was treated by a bronchial artery embolization (BAE) procedure. The results of detailed examinations diagnosed him as pulmonary hypertension and pulmonary arterial embolism. Therefore, he was referred to our hospital. Preoperative hemodynamic data was as follows, mean pulmonary arterial pressure (mPpa); 55 mmHg, pulmonary vascular resistance (PVR); 982 dyne sec $cm^{-5}$. By computed tomographic (CT) scan, lung perfusion scan, and pulmonary angiography, chronic pulmonary embolism was detected. He was diagnosed as CTEPH and pulmonary endarterectomy (PEA) was performed by Dr. Masahisa Masuda at the Chiba Medical Center, Japan. After the surgery, the hemodynamic improved as follows, mPpa; 17 mmHg, PVR; 202 dyne sec $cm^{-5}$. Resected organized thrombi were investigated pathologically. Pathological diagnosis was atherosclerosis-intima fibrosis of pulmonary arteries with partial recanalization, which was the typical finding of chronic pulmonary thrombosis, and no malignant cell was detected. Although it's already been five years or more after the operation, he has no intimal sarcoma now.

### Cell isolation

One part of resected organized thrombi was investigated pathologically and the other part was done in this study. At the second passage of the myofibroblast-like cells obtained following incubation of the endarterectomized tissues, pleomorphic cells (called sarcoma-like cells (SCLs)), were isolated, probably by chance. The details of the cell isolation have been described previously [5].

### Cell lines and reagents

A549 cells (a human lung carcinoma cell line) were purchased from Takara Biomedical (Ohtsu, Shiga, Japan). SCLs were incubated using endothelial cell growth medium supplemented with 5% fetal bovine serum (FBS) and growth factors (EGM-2) (Lonza Inc, Allendale, NJ, USA) at 37°C in 5% $CO_2$ in air in a humidified incubator. A549 cells were cultured using RPMI 1640 media (Life Technologies, Carlsbad, CA, USA) with 5% FBS. In order to exclude the effects of several growth factors present in the EGM, endothelial cell basal medium-2 (EBM-2) (Lonza Inc, Allendale, NJ, USA), with only 5% FBS, was used in some experiments. Batimastat, a synthetic matrix metalloproteinase inhibitor, was purchased from Merck Millipore (Darmstadt, Germany). Batimastat was diluted in dimethyl sulfoxide, stored at −20°C and was prepared just before use in experiments. The antibodies used for the immunohistochemical studies were: mouse anti-vimentin (1:200, Dako, Carpinteria, CA, USA), mouse anti-human, rabbit anti-von Willebrand factor (factor VIII) (1:1,000, Dako), rabbit anti-CD31 (1:200, Abcam, Cambridge, UK), anti-MMP-14 (1:200), rabbit anti-MMP-2 (1:200, Abcam), mouse anti-CD44 (1:100, Abcam), an anti-mouse IgG conjugated with Alexa-488 fluorescent dye (1:200, Molecular Probes, Tokyo, Japan), an anti-rabbit IgG conjugated with Alexa-488 fluorescent dye (1:200, Molecular Probes), rabbit anti-MMP-14 (1:200, Abcam), MMP-2 (1:100, Abcam) and polyclonal biotinylated goat anti-rabbit immunoglobulins (1:500, Dako). The antibodies used in the Western blot analysis were: MMP-14 antibodies (1:500, Abcam), MMP-2 antibodies (1:500, Abcam), β-actin antibodies (1:1000, Cell Signaling Technology, Boston, MA, USA) and stabilized goat anti-rabbit IgG (H+L), which was peroxidase conjugated (ThermoScientific, Massachusetts, MA, USA).

### PCR array

In order to confirm the different RNA expression levels between SCLs as mesenchymal malignant tumor cells and A549 as epithelial cancer cells, a PCR array analysis focusing on the adhesion molecules was performed. Our previous study had demonstrated that there was increased mRNA expression of MMPs in SCLs in comparison to A549 cells [5]. Therefore, a PCR array was used to confirm the precise expression levels of various MMPs. The $RT^2$ Profiler PCR Array (SABiosciences, Frederick, USA) was used for this purpose. The details of this protocol have been described previously [5].

### Invasion and migration assay

The BD BioCoat FluoroBlok Invasion System (24-multiwell) was used to assess the invasion and migration of SCLs with or without batimastat treatment. In order to exclude the effects of additives, including growth factors, SCLs were incubated with the EBM-2 for three days. Then, $2.5\times10^5$ pretreated SCLs were seeded to each upper well of the kit with serum free medium. The medium added to each lower well was as follows: EBM-2 containing 5% FBS and dimethyl sulfoxide (the same quantity as the solvent used for dissolving 10 μM batimastat) (control group), 5% FBS and 1 μM batimastat (1 μM batimastat group) or 5% FBS and 10 μM batimastat (10 μM batimastat group). The kits were incubated at 37°C in 5% $CO_2$, in a humidity-controlled incubator for 16 hours. The fixation, staining and quantification of the invaded cells were described previously [5].

### Three-dimensional cultures

BD Matrigel™ Basement Membrane Matrix Growth Factor Reduced (BD Falcon, USA) was used for three-dimensional cultures. This experiment was conducted in accordance with the recommended "thin-gel method". Matrigel was gently thawed in a 4°C refrigerator. A 50 μl aliquot of Matrigel was added thinly to each wells of a 24-well plate. The plates were incubated in a 37°C incubator for 15 minutes. After that, 20 μl of Matrigel and $5\times10^4$ cells suspended in 1000 μl medium were mixed and seeded into each well. The findings in SCLs and A549 were investigated. In order to study the effects of batimastat, 1 μM or 10 μM of batimastat were added to the EBM-2 media. Finally, the plates were incubated at 37° in a 5% $CO_2$ in air in a humidified incubator for different periods of time.

### Western blot analysis

The cultured cells on the dishes were washed, homogenized in lysis buffer (20 mM Tris-HCl, pH 8.0, 1 mM EDTA, 1 mM $NaN_3$, 1 mM DTT, 150 mM NaCl, 0.5% Triton-X, phosphatase inhibitor cocktail (SIGMA P5726)), and centrifuged at 10,000×g for 5 min. The protein concentrations of these supernatants were measured by the Bradford method (Bio-Rad protein assay; Nippon Bio-Rad Laboratories, Tokyo, Japan). Protein samples (2 μg) were separated on 10% Tris-glycine gels (Invitrogen Japan, Tokyo, Japan) and transferred to nitrocellulose membranes (Invitrogen Japan, Tokyo, Japan). Membranes were blocked with 5% non-fat dried milk in PBS containing 0.5% Tween20 for 1 hour at 4°C,

and were then incubated with primary antibodies. The membranes were incubated with peroxidase-conjugated secondary antibodies for 1 hour at room temperature. Chemiluminescence was detected by a LAS-1000 instrument (Fuji Film, Tokyo, Japan). Signals were quantified using the Fuji Image Gauge software program (ver. 3.0, Fuji Film, Tokyo, Japan).

### Cell culture with a matrix metalloproteinase inhibitor

SCLs were incubated with growth factor-free medium for three days. They were then washed and trypsinized. A total of $1\times10^5$ cells were added to fibronectin-coated dishes. They were incubated with the EBM-2 containing DMSO (control group), 1 μM batimastat (1 μM batimastat group) or 10 μM batimastat (10 μM batimastat group) at 37° in a 5% $CO_2$ in air in a humidified incubator for 24 hours, 48 hours or 72 hours. At the appropriate times, the cell numbers were counted.

### Intravascular and subcutaneous tumor formation

Icr/scid mice were purchased from Nihon Clea. SCLs incubated in EGM media were trypsinized, and $2\times10^6$ cells were injected intravenously into the mice. Twenty-eight days after injection, the mice were sacrificed, and various organs, including the lungs, were resected. These tissues were pathologically investigated. A total of $1\times10^6$ cells were injected subcutaneously into the Icr/scid mice. Then 40 mg/kg batimastat was injected intraperitoneally once a day from day 3 to day 13. On day 14, they were sacrificed, and the subcutaneous tumors were resected. Tumors were weighed and pathologically examined.

### Immunohistochemistry

Samples were fixed in 10% buffered formalin, paraffinized and sliced at 1.5 μm thick. Antigen retrieval was performed using pH 6.0 citrate buffer (Abcam # 64214) for the deparaffinized slices. Sections were blocked with 2% normal goat serum, PBS(-) and 0.1% Tween20 for 30 min at room temperature. They were then incubated with the primary antibodies for 1 hour at 4°C and with secondary antibodies for 30 minutes at room temperature. The avidin-biotin-peroxidase complex method with peroxidase streptavidin (Nichirei #426062, Tokyo, Japan) and the DAB substrate kit (Abcam ab64238) was performed.

### Statistical analysis

The PCR array data were analyzed by a web-based software program, the $RT^2$ Profiler PCR Array Data Analysis, version 3.5 (http://pcrdataanalysis.sabiosciences.com/pcr/arrayanalysis.php). The other data were analyzed using the useful and reliable statistical software, EZR on R commander [7] (ver.1.03, provided on the site of Division of Hematology, Saitama Medical Center, Jichi Medical University (http://www.jichi.ac.jp/saitama-sct/SaitamaHP.files/statmedEN.html)). At least three samples were used for the statistical analyses. We considered that the differences were significant for values of $p<0.05$.

## Results

### MMPs expression

The PCR array analysis showed that there was increased mRNA expression for MMP-2, MMP-14 and MMP-16 in the SCLs in comparison to the A549 cells (Table 1, Figure 1). In addition, decreased expression of MMP-7 mRNA was confirmed in SCLs in comparison to the A549 cells (Table 1, Figure 1). A Western blot analysis revealed that the MMP-14 protein expression in SCLs was higher than that in A549 (Figure 2A). There was no obvious difference in the protein expression of MMP-2 and MMP-14 in the SCLs incubated in the media with (EGM) or without (EBM) growth factors (Figure 2A).

### Immunohistochemistry

Immunohistochemical staining showed that SCLs were positive for vimentin (Figure 3A), MMP-14 (Figure 3F), MMP-2 (Figure 3G) and CD44 (Figure 3H) which is a cell-surface glycoprotein involved in cell adhesion and migration. However, endothelial cell markers, including Factor VIII (Figure 3B) and CD31 (Figure 3C), a smooth muscle cell marker, α-SMA (Figure 3D) and desmin (Figure 3E) were negative. C.B-17/Icr-scid/scidJcl mice which were intravenously injected with SCLs developed tumors which grew along the intimal surface of the

**Table 1.** Expressions of matrixmetalloproteinase of SCLs on PCR array.

| Description | Gene symbol | Public ID | Fold Change (95%CI) | p-value |
|---|---|---|---|---|
| Matrix metallopeptidase 1 (interstitial collagenase) | MMP1 | NM_002421 | 1.2872 (0.00001–2.77) | N.S. |
| Matrix metallopeptidase 2 (gelatinase A, 72 kDa gelatinase, 72 kDa type IV collagenase) | MMP2 | NM_004530 | 25.9049 (0.00001–60.45) | <0.05 |
| Matrix metallopeptidase 3 (stromelysin 1, progelatinase) | MMP3 | NM_002422 | −0.4998 (−1.10– −0.00001) | N.S. |
| Matrix metallopeptidase 7 (matrilysin, uterine) | MMP7 | NM_002423 | −0.037 (−0.06– −0.01) | <0.00005 |
| Matrix metallopeptidase 8 (neutrophil collagenase) | MMP8 | NM_002424 | −0.4566 (−1.11– −0.00001) | N.S. |
| Matrix metallopeptidase 9 (gelatinase B, 92 kDa gelatinase, 92 kDa type IV collagenase) | MMP9 | NM_004994 | 0.9158 (0.00001–2.04) | N.S. |
| Matrix metallopeptidase 10 (stromelysin 2) | MMP10 | NM_002425 | 1.1935 (0.00001–3.16) | N.S. |
| Matrix metallopeptidase 11 (stromelysin 3) | MMP11 | NM_005940 | 0.8688 (0.00001–2.01) | N.S. |
| Matrix metallopeptidase 12 (macrophage elastase) | MMP12 | NM_002426 | 1.3401 (0.24–2.44) | N.S. |
| Matrix metallopeptidase 13 (collagenase 3) | MMP13 | NM_002427 | 1.5681 (0.05–3.09) | N.S. |
| Matrix metallopeptidase 14 (membrane-inserted) | MMP14 | NM_004995 | 90.8284 (27.28–154.38) | <0.01 |
| Matrix metallopeptidase 15 (membrane-inserted) | MMP15 | NM_002428 | 2.573 (0.93–4.22) | N.S. |
| Matrix metallopeptidase 16 (membrane-inserted) | MMP16 | NM_005941 | 7.9291 (2.24–13.62) | <0.05 |

doi:10.1371/journal.pone.0087489.t001

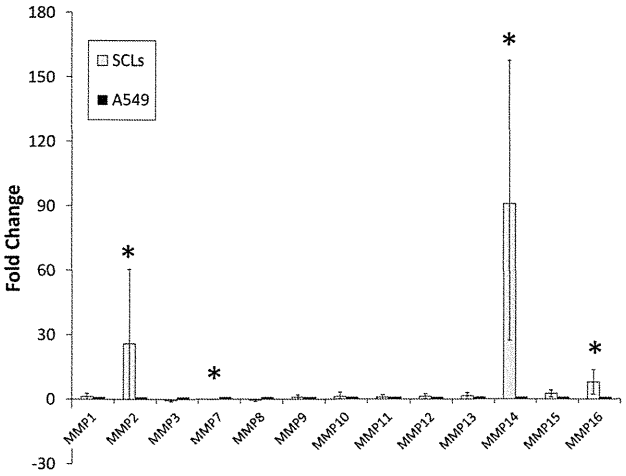


**Figure 1. The results of the PCR array analysis focused on the matrix metalloproteinases (MMPs) of SCLs.** The expression levels of MMP-14 and MMP-2 of SCLs were higher than those of A549 cells, while the level of MMP-7 was lower. These data were analyzed by a web-based software program (the $RT^2$ Profiler PCR Array Data Analysis, version 3.5). Error bars showed 95% Confidencial intervals. (* p-value < 0.05 versus A549, n = 5)
doi:10.1371/journal.pone.0087489.g001

pulmonary arteries (Figures 4A, 4B). The peripheral lesions of tumors seemed to be a cell-rich layer, while the center of the tumors was a necrotic zone (Figure 4B). The cells in the tumor were positive for MMP-14 and MMP-2 (Figures 4C, 4D).

## Three-dimensional culture

The three-dimensional culture system was employed to confirm the SCL proliferation under *in vivo* conditions, which could make the cells grow in an environment that more closely resembled their normal condition. SCLs, as mesenchymal neoplastic cells, formed aligned structures as tube-like networks during the 12-hour incubation period (Figure 5A). In contrast, the A549 adenocarcinoma cells did not organize themselves into aligned structures (Figure 5B).

## Effects of a synthetic matrix metalloproteinase inhibitor, batimastat

In order to confirm the role of MMPs in the growth and death of SCLs, the cells were incubated in the EBM-2 media with batimastat. Although batimastat did not suppress the protein expression of MMP-14 or MMP-2 (Figures 2B-2D), this reagent did suppress the number of proliferating SCLs (Figure 6A). Moreover, the invasion assay demonstrated that batimastat decreased the invasion of SCLs (Figure 6B), and the three-dimensional culture showed that it prevented these cells from organizing themselves into aligned tube-like structures (Figures 5C, 5D).

To investigate the effects of batimastat on the tumorigenesis of SCLs in Icr/scid mice, $1\times10^6$ cells were injected subcutaneously, and were then treated intraperitoneally with 40 mg/kg batimastat once a day from day 3 to day 13. On day 14, the resected subcutaneous tumors were weighed, and there was a significant difference between the control (n = 6) (Figure 7A) and batimastat (n = 4) (Figure 7B) groups (control group 267.5±113.8 mg vs batimastat group 112.9±56.4 mg, $p<0.05$) (Figure 7C). There were no significant differences in the body weight between the groups on the day of SCLs injection (day 0: control group

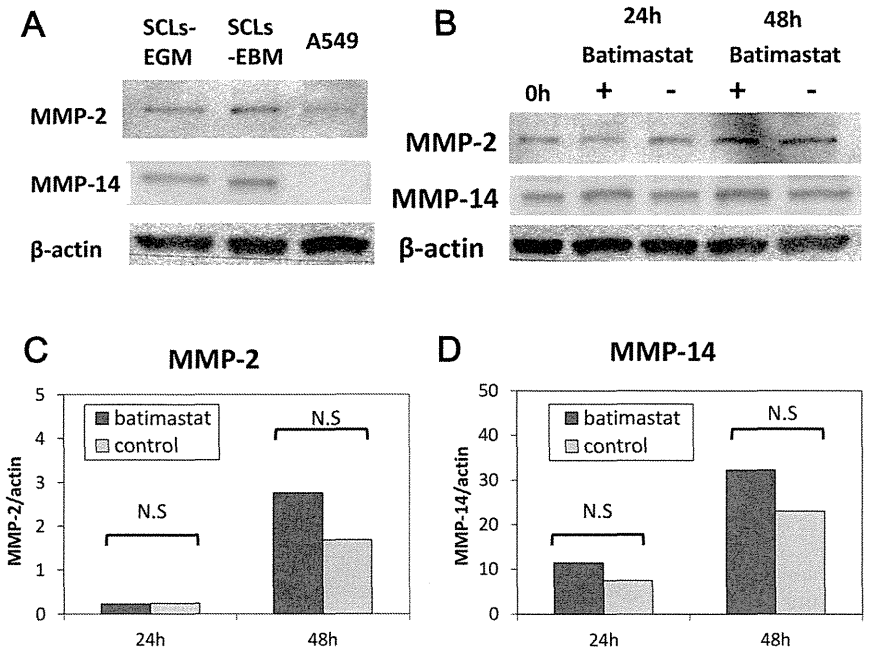


**Figure 2. The results of the Western blot analysis.** (A) The Western blot analysis revealed that the MMP-14 protein expression in SCLs was higher than that in A549 cells. There was no significant difference in the protein expression of MMP-14 in SCLs incubated in the media with or without growth factors. (B) Batimastat did not suppress the SCLs' expression of the MMP-14 and MMP-2 proteins. (C)(D) The band signal strength of MMP-14 (c) and MMP-2 (d) expressed as a ratio to beta-actin. No significant differences in the signal strength were recognized 24 hours and 48 hours after batimastat exposure between the batimastat and control groups. ("N.S." showed no significant difference between two groups analyzed by Student's t-test.)
doi:10.1371/journal.pone.0087489.g002

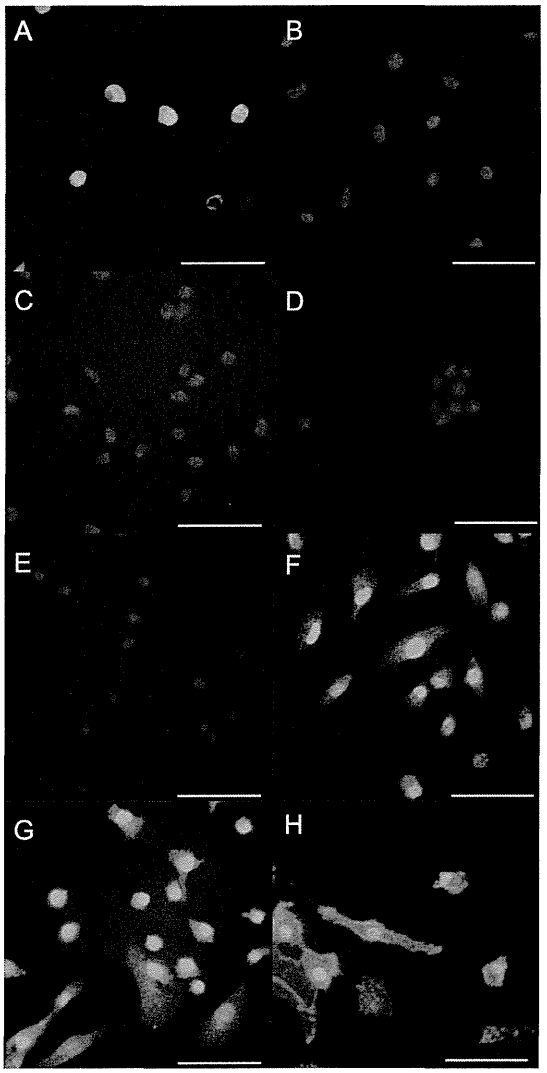


**Figure 3. The results of the immunohistochemical analysis of the SCLs.** The SCLs were positive for vimentin (A), MMP-14 (F), MMP-2 (G) and CD44 (H). In contrast, the staining for α-SMA (B), VWF (C), CD31 (D) and desmin (E) was negative. (Scale bars show 50 μm.)
doi:10.1371/journal.pone.0087489.g003

20.6±1.0 g vs batimastat group 21.7±0.8 g, $p>0.05$) or on the first day of batimastat injection (day 3: control group 21.7±0.9 g vs batimastat group 22.3±0.8 g, $p>0.05$). On day 14, there was a significant difference in the body weight between the groups (control group 20.7±0.8 g vs batimastat group 22.2±0.7 g, $p<0.05$).

## Discussion

The present study demonstrated that there was an increased expression of MMP-14 in SCLs (Figures 1–4) and that the blockade of the MMPs cascades by batimastat suppressed the pathobiological activities of SCLs in *in vivo* and *in vitro* experiments (Figures 5–7). MMPs are a group of endopeptidases biochemically characterized by their dependence on zinc at the active site [8,9]. MMPs degrade most components of the extracellular matrix (ECM) and are considered to have an important role in various biological processes in cells, such as proliferation, apoptosis, invasion, differentiation and angiogenesis [8,9]. Generally, MMPs

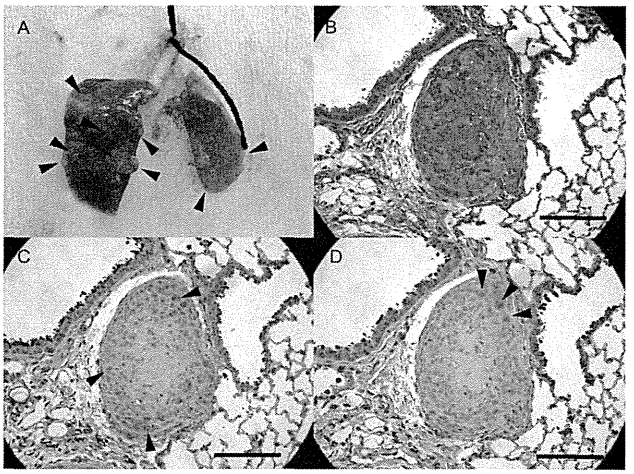


**Figure 4. Tumors which grew along the intimal surface of the pulmonary arteries.** (A) A resected lung from a mouse. SCID mice were sacrificed 28 days after the injection of SCLs. Many nodules were located on the surface of the lungs. Arrow heads showed some of these nodules. (B) HE staining showed that the tumors were composed of a central area with necrosis and a peripheral zone filled with SCLs. (C) Immunohistochemical staining for MMP-14 revealed that the peripheral area of tumors was positive for MMP-14, and the central necrotic area was negative for MMP-14. (D) Immunohistochemical staining for MMP-2 showed that MMP-2 was weakly positive in the peripheral zone. (Scale bars show 100 μm.)
doi:10.1371/journal.pone.0087489.g004

are divided into two groups; secretion-type and membrane-type (MT). Because of its cell surface expression, MMP-14 is called MT1-MMP [10,11,12]. MMP-14 has many functions, including ECM degradation, the activation of MMP-2 and MMP-13 [11,13] and the cleavage of cell surface receptors, such as CD44 [10,11,13]. Therefore, because MMP-14 is a modulator of the pericellular microenvironment [10], it is thought to have critical

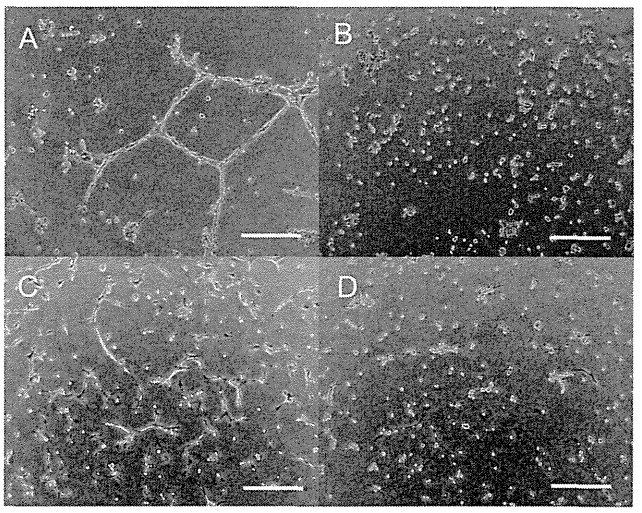


**Figure 5. The findings of the three-dimensional culture of SCLs.** Cells were incubated for 12 hours (A and B) or 24 hours (C and D). SCLs proliferated linearly and formed tube-like structures and network-like structures within Matrigel (A), but the A549 (lung adenocarcinoma) cells formed no network structures (B). SCLs incubated with EBM-2 also formed the tube-like structures in the Matrigel (C). Exposure to 10 μM batimastat inhibited the formation of the three-dimensional structures (D). (Scale bars show 300 μm.)
doi:10.1371/journal.pone.0087489.g005

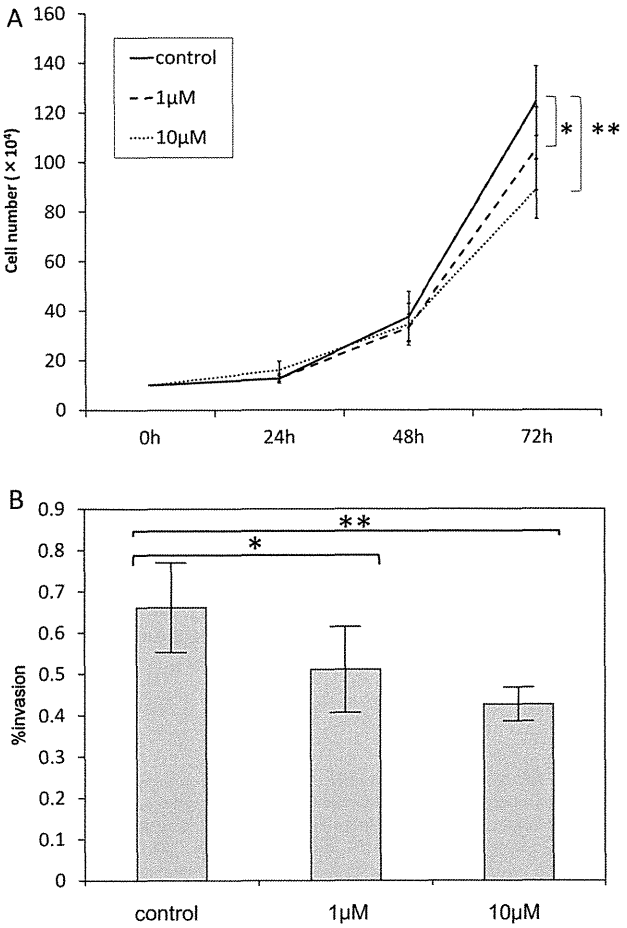


**Figure 6. Batimastat suppressed the biological activities of SCLs in *in vivo* studies.** (A) Batimastat, a synthetic matrix metalloproteinase inhibitor, suppressed the proliferation of SCLs 72 hours after incubation with batimastat. The number of SCLs that survived following the culture with batimastat was lower than that in the control group. (* p-value <0.05, **p-value<0.01 versus control group, by Student's t-test, n = 6). (B) The invasion assays revealed that the SCLs incubated with batimastat were less invasive than those in the control group. (* p-value <0.05 versus control group, **p-value<0.01 versus control group, by Student's t-test, n = 8)
doi:10.1371/journal.pone.0087489.g006

roles in controlling the invasive and metastatic capabilities of malignant cells [10,11].

Batimastat is a synthetic MMP inhibitor, and the depressant action of this agent is biochemically explained by the binding of a hydroxamate to the zinc ion in the active center of MMPs [14]. In this study, batimastat inhibited the proliferation of SCLs (Figure 6A). Some studies, however, reported that batimastat did not suppress the proliferation of malignant cells [15,16]. Zervos et al. showed that anti-proliferative effect of this drug on human pancreatic adenocarcinoma cells was apparent in a high dose of this drug [17], indicating that anti-proliferative effect of this drug might be in a dose-dependent manner. This supports our results on Figure 6. Moreover, batimastat suppressed invasive activity of SCLs in the present study. Ueda et al. also reported that the invasive fibrosarcoma cells were suppressed by 10 μM batimastat [18]. In truth, MMP-14 is supposed to play a critical role on cell invasion activity through effect as the degeneration of extracellular matrix [12,19].

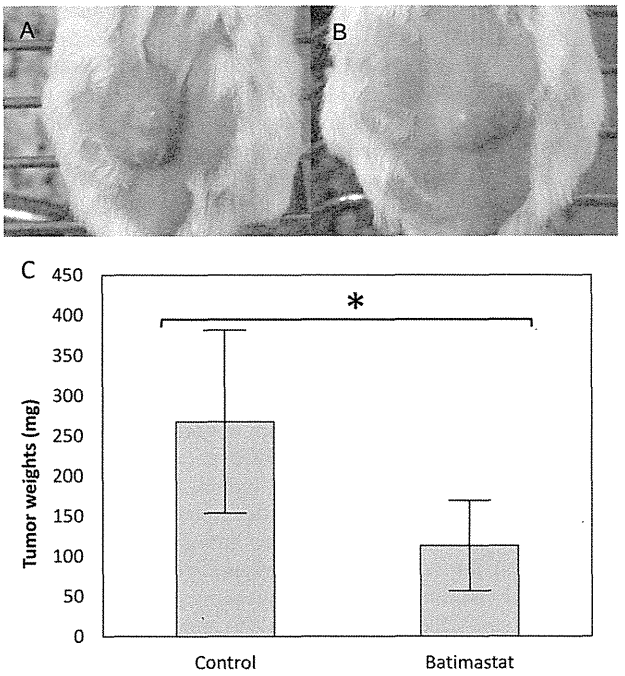


**Figure 7. Batimastat suppressed the growth of SCLs in xenograft models.** Subcutaneous tumors were formed on the backs of the mice in the control group (A) and batimastat group (B). It was revealed that there were significant differences in the tumor weights between the control group (n = 6) and batimastat group (n = 4) (C). (* p-value <0.05, versus control group, by Student's t-test)
doi:10.1371/journal.pone.0087489.g007

Kadono et al. reported that batimastat inhibited the formation of three-dimensional structures by fibrosarcoma cells [20], as well as their migration and adhesion [21]. In this study, SCLs formed tube-like or network-like structures in the three-dimensional culture, and batimastat prevented the formation of these structures by the SCLs (Figure 5). This result supported the findings in the previous report. However, A549 cells could not form the tube-like or network-like structures in the three-dimensional culture (Figure 5B), and these differences are likely attributable to the fact that the SCLs were mesenchymal cells which had originated from the pulmonary vasculature, while A549 cells are cancer cells of epithelial origin. Moreover, the mRNA and protein expression levels of MMP14 in SCLs were higher than those in A549 cells (Figures 1 and 2A), leading to a higher potential for the degradation of the extracellular matrix by the SCLs, which might explain the results of the three-dimensional culture experiments. In fact, there was a previous report that described that the MMP-14 expression level was strongly related to the formation of three-dimensional structures by malignant cells [22].

The Western blot analysis demonstrated that the protein expression levels of MMP-2 and MMP-14 did not decrease, but were actually slightly increased after the batimastat treatments (Figure 2), indicating that, as expected based on its putative mechanism of action, batimastat could suppress only the activities of MMPs, rather than affecting their protein expression levels. In addition, the positive feedback induced by the blockade of the activity of MMPs might have led to the increased expression of MMP-2 and MMP-14 in these cultures.

In the present study, batimastat could suppress the development of subcutaneous tumors in Icr/scid mice (Figure 7), supporting the previous reports showing the effectiveness of this reagent for controlling the growth of other tumors, such as ovarian carcinoma

[23], breast cancer [24], pancreatic cancer [17], a human colon cancer model [25] and a metastatic human colon carcinoma model [15]. However, the details of the fundamental mechanisms by which batimastat prevents tumor growth remain to be elucidated. In this study, batimastat could suppress the enlargement of SCL tumors and maintain the weight of mice. It is known that maintenance of the body weight by patients with malignant tumors contributes to a better quality of life [26]. Therefore, it was supposed that both the tumor growth suppression and the effect on the mouse body weight were important for the anti-cancer effects of batimastat.

The findings from this study and the previous study [5] suggest that the behavior and the characteristic of SCLs resemble those of pulmonary intimal sarcoma cells. Clinically, intimal sarcoma is an extremely rare disease, and to the best of our knowledge, there have been no cell lines isolated from intimal sarcoma tissues. Pulmonary intimal sarcoma is believed to originate from the mesenchymal cells present within the intimal layer of pulmonary arteries [27]. Vasuli et al. previously described the immunohistochemical characteristics of pulmonary intimal sarcoma tissues, indicating that the cells of intimal sarcoma were positive for the mesenchymal cell marker, vimentin, negative for the endothelial cell markers von-Willebrand factor (VWF) and CD31, and for the smooth muscle cell marker, α-smooth muscle actin [28]. In addition, this study also described that the undifferentiated intimal sarcoma cells were positive for mesenchymal stem cell markers, such as RUNX-1 or CD44 [28]. As described above, the SCLs in the present study were positive for vimentin and CD44 and negative for CD31 and VWF, α-smooth muscle actin and desmin (Figure 3). SCLs had some characteristics which resemble those of pulmonary intimal sarcoma. However, SCLs were derived from only one patient with CTEPH and the isolation of SCLs was not reproducible. CTEPH and pulmonary initimal sarcoma are completely different diseases and it remains unknown how and why this only one cell line represents characteristics of initimal sarcomas.

In conclusion, this study suggested that MMPs had critical roles on the pathological activities of SCLs and that batimastat might have anti-proliferative and anti-invasive effect on these cells.

## Acknowledgments

All authors read and approved the final manuscript. We thank Dr. Yoshitoshi Kasuya for the important advice about our study.

## Author Contributions

Conceived and designed the experiments: TJ SS. Performed the experiments: TJ MT M. Maruoka SK. Analyzed the data: TJ SS NT. Wrote the paper: TJ SS M. Masuda NT KT.

## References

1. Firth AL, Yao W, Ogawa A, Madani MM, Lin GY, et al. (2010) Multipotent mesenchymal progenitor cells are present in endarterectomized tissues from patients with chronic thromboembolic pulmonary hypertension. Am J Physiol Cell Physiol. 298:C1217–1225.
2. Yao W, Firth AL, Sacks RS, Ogawa A, Auger WR, et al. (2009) Identification of putative endothelial progenitor cells (CD34+CD133+Flk-1+) in endarterectomized tissue of patients with chronic thromboembolic pulmonary hypertension. Am J Physiol Lung Cell Mol Physiol. 296:L870–878.
3. Maruoka M, Sakao S, Kantake M, Tanabe N, Kasahara Y, et al. (2012) Characterization of myofibroblasts in chronic thromboembolic pulmonary hypertension. Int J Cardiol. 159:119–127.
4. Hanahan D, Weinberg RA. (2011) Hallmarks of cancer: the next generation. Cell. 144:646–674.
5. Jujo T, Sakao S, Kantake M, Maruoka M, Tanabe N, et al. (2012) Characterization of sarcoma-like cells derived from endarterectomized tissues from patients with CTEPH and establishment of a mouse model of pulmonary artery intimal sarcoma. Int J Oncol. 41:701–711.
6. Bloomberg RD, Butany JW, Cusimano RJ, Leask RL. (2003) Primary cardiac sarcoma involving the pulmonary artery and valve. Can J Cardiol 19: 843–847.
7. Kanda Y. (2013) Investigation of the freely available easy-to-use software 'EZR' for medical statistics. Bone Marrow Transplant. 48:452–458.
8. Rasmussen HS, McCann PP. (1997) Matrix metalloproteinase inhibition as a novel anticancer strategy: a review with special focus on batimastat and marimastat. Pharmacol Ther. 75:69–75.
9. Woessner JF. (1991) Matrix metalloproteinases and their inhibitors in connective tissue remodeling. FASEB J. 5:2145–2154
10. Sato H, Takino T, Miyamori H. (2005) Roles of membrane-type matrix metalloproteinase-1 in tumor invasion and metastasis. Cancer Sci. 96:212–217.
11. Chakraborti S, Mandal M, Das S, Mandal A, Chakraborti T. (2003) Regulation of matrix metalloproteinases. Mol Cell Biochem. 253:269–285.
12. Sato H, Takino T, Okada Y, Cao J, Shinagawa A, et al. (1994) A matrix metalloproteinase expressed on the surface of invasive tumour cells. Nature. 370:61–65.
13. Itoh Y, Seiki M. (2006) MT1-MMP: a potent modifier of pericellular microenvironment. J Cell Physiol. 206:1–8.
14. Botos I, Scapozza L, Zhang D Liotta LA, Meyer EF. (1996) Batimastat, a potent matrix mealloproteinase inhibitor, exhibits an unexpected mode of binding. Proc Natl Acad Sci U S A 93:2749–2754.
15. Watson SA, Morris TM, Robinson G, Crimmin MJ, Brown PD, et al. (1995) Inhibition of organ invasion by the matrix metalloproteinase inhibitor batimastat (BB-94) in two human colon carcinoma metastasis models. Cancer Res. 55:3629–3633.
16. Chirivi RG, Garofalo A, Crimmin MJ, Bawden LJ, Stoppacciaro A, et al. (1994) Inhibition of the metastatic spread and growth of B16-BL6 murine melanoma by a synthetic matrix metalloproteinase inhibitor. Int J Cancer. 58:460–464.
17. Zervos EE, Norman JG, Gower WR, Franz MG, Rosemurgy AS. (1997) Matrix metalloproteinase inhibition attenuates human pancreatic cancer growth in vitro and decreases mortality and tumorigenesis in vivo. J Surg Res 69:367–371.
18. Ueda J, Kajita M, Suenaga N, Fujii K, Seiki M. (2003) Sequence-specific silencing of MT1-MMP expression suppresses tumor cell migration and invasion: importance of MT1-MMP as a therapeutic target for invasive tumors. Oncogene. 22:8716–8722.
19. Sato H, Takino T. (2010) Coordinate action of membrane-type matrix metalloproteinase-1 (MT1-MMP) and MMP-2 enhances pericellular proteolysis and invasion. Cancer Sci. 101:843–847.
20. Kadono Y, Shibahara K, Namiki M, Watanabe Y, Seiki M, et al. (1998) Membrane type 1-matrix metalloproteinase is involved in the formation of hepatocyte growth factor/scatter factor-induced branching tubules in madin-darby canine kidney epithelial cells. Biochem Biophys Res Commun. 251:681–687.
21. Takino T, Miyamori H, Watanabe Y, Yoshioka K, Seiki M, et al. (2004) Membrane type 1 matrix metalloproteinase regulates collagen-dependent mitogen-activated protein/extracellular signal-related kinase activation and cell migration. Cancer Res. 64:1044–1049.
22. Hotary KB, Allen ED, Brooks PC, Datta NS, Long MW, et al. (2003) Membrane type I matrix metalloproteinase usurps tumor growth control imposed by the three-dimensional extracellular matrix. Cell. 114:33–45
23. Davies B, Brown PD, East N, Crimmin MJ, Balkwill FR. (1993) A synthetic matrix metalloproteinase inhibitor decreases tumor burden and prolongs survival of mice bearing human ovarian carcinoma xenografts. Cancer Res. 53:2087–2091.
24. Sledge GW Jr, Qulali M, Goulet R, Bone EA, Fife R. (1995) Effect of matrix metalloproteinase inhibitor batimastat on breast cancer regrowth and metastasis in athymic mice. J Natl Cancer Inst. 87:1546–1550.
25. Wang X, Fu X, Brown PD, Crimmin MJ, Hoffman RM. (1994) Matrix metalloproteinase inhibitor BB-94 (batimastat) inhibits human colon tumor growth and spread in a patient-like orthotopic model in nude mice. Cancer Res. 54:4726–4728.
26. Doyle C, Kushi LH, Byers T, Courneya KS, Demark-Wahnefried W, et al. (2006) Nutrition and physical activity during and after cancer treatment: an American Cancer Society guide for informed choices. CA Cancer J Clin. 56:323–353.
27. Altman NH, Shelley WM. (1973) Primary intimal sarcoma of the pulmonary artery. Johns Hopkins Med J. 133:214–222.
28. Vasuri F, Resta L, Fittipaldi S, Malvi D, Pasquinelli G. (2012) RUNX-1 and CD44 as markers of resident stem cell derivation in undifferentiated intimal sarcoma of pulmonary artery. Histopathology. 61:737–743.

# PVODにおける画像所見の特徴

木曽啓祐* 東 将浩*

Summary 本稿ではPVODにおける各種放射線画像所見の特徴について取り上げる。胸部X線写真や単純CTでは心拡大・肺動脈拡張などの右心系負荷所見が認められ，HRCTでは小葉中心性に分布するすりガラス様陰影や小葉間隔壁の肥厚が多く認められる。肺血流シンチグラフィーでは全体的に淡い不均一性を示すほか，上葉の血流低下も多く見られる。以上のような特徴を総合的にとらえることでPVODの早期診断につなげることができればと願っている。

Key words 肺静脈閉塞症，胸部X線写真，CT，肺血流シンチグラフィー／pulmonary veno-occlusive disease（PVOD），chest X-ray film, CT, lung perfusion scintigraphy

## はじめに

肺静脈閉塞症（pulmonary veno-occlusive disease：PVOD）は他項で述べられているとおり，肺高血圧を呈する原因疾患の中でも非常にまれな疾患とされており，正確な頻度は不明ではあるが特発性肺動脈性肺高血圧症の約10%程度と報告されている。さらに，近年の肺高血圧症に対する薬物療法の進歩により，肺高血圧症全体では予後の改善が見られているにもかかわらず，本疾患は依然難治性で予後不良であることも知られており，肺移植が唯一の根本治療法とされている。また，その診断は病理組織検査で確定されるが，それ以外の検査による早期診断は困難であることが多く，剖検により初めて診断が明らかになるケースも多く，生前診断が難しいことでも知られている。

そこで，今回はPVODにおける画像診断について胸部X線写真・CT・肺血流シンチグラフィーを取り上げ，その画像所見の特徴やほかの肺高血圧症起因疾患との相違点・鑑別点などについて解説したい。

## 胸部X線写真

胸部X線写真は初診検査から経過観察まで最も多用される検査の一つであるが，その画像所見は重症肺高血圧を反映して右心系負荷所見である「心拡大」・「肺動脈拡張」が認められるのは当然のこと，加えてPVODは肺

* 国立循環器病研究センター放射線部（〒565-8565 大阪府吹田市藤白台5-7-1）

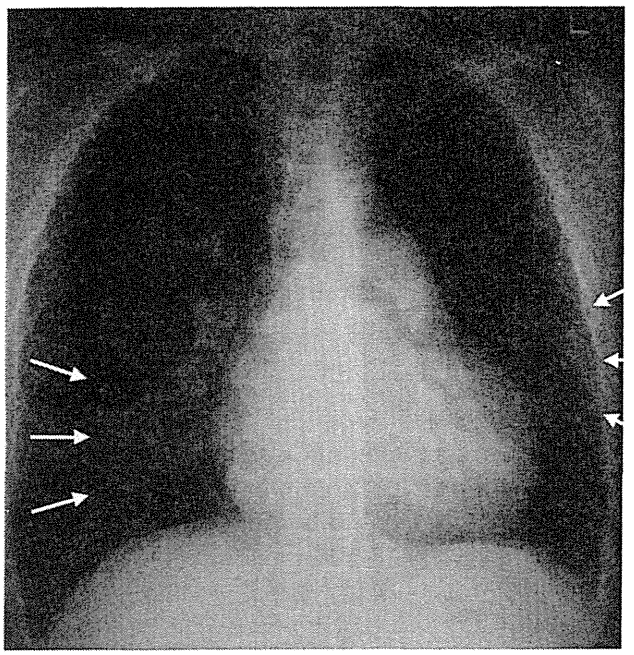

図 1　PVOD の胸部 X 線写真
心拡大および肺動脈の拡張のほかに右下肺野や左中肺野に淡いすりガラス様陰影を認める（矢印）。

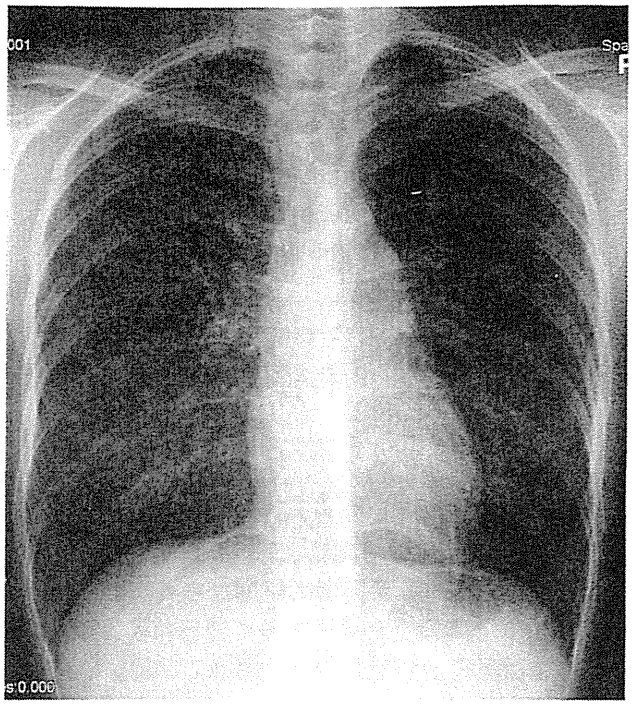

図 2　IPAH の胸部 X 線写真
心拡大は目立たないが，左第 2 弓の突出を認める。
さらに，肺門部の血管影は目立つ一方で末梢の血管影は目立たず，末梢肺野領域は明るい印象を受ける。

水腫を来す頻度が高いことを反映して「Kerley B line」も比較的頻度高く認められると報告されている。その他にもすりガラス様陰影などの間質影の増強が見られる症例が多いことも報告されている。

一方，同じく肺高血圧原因疾患である特発性肺動脈性肺高血圧症（idiopathic pulmonary artery hypertension：IPAH）では末梢肺血管陰影が減少し，肺野末梢が明るく見えることが特徴とされ，PVOD との相違点の 1 つとされている。

図 1 に PVOD 症例の胸部 X 線写真を示すが，先述の通り心拡大・両側肺動脈拡張が見られるほか，両肺野にすりガラス様陰影も認められる。

一方，図 2 には IPAH 症例の胸部 X 線写真を示す。本文に記したように中枢側の肺動脈の拡張は認められるが，末梢の肺血管陰影は乏しくその結果，肺野末梢が明るく見えている。

## CT

通常の CT では胸部 X 線写真同様に心拡大・肺動脈拡張が認められ，さらに肺高血圧に起因した右室負荷を反映して右室の拡大と心室中隔の扁平化ないしは左室側への圧排を認めることが多い。さらに，リンパ節の腫大の頻度も IPAH と比較すると高いことが報告されている。その他に胸水や心嚢水が認められる頻度も高いと言われる。

図 3，4 に PVOD 症例の単純 CT 像（縦隔条件）を提示するが，肺動脈の主幹部から左右肺動脈に至るまで著明な拡大を認め（図 3），心臓に関しても著明な右室拡大と心室中隔の左室側への圧排を認める（図 4）。

また，2 mm 以下の薄いスライス厚で拡大

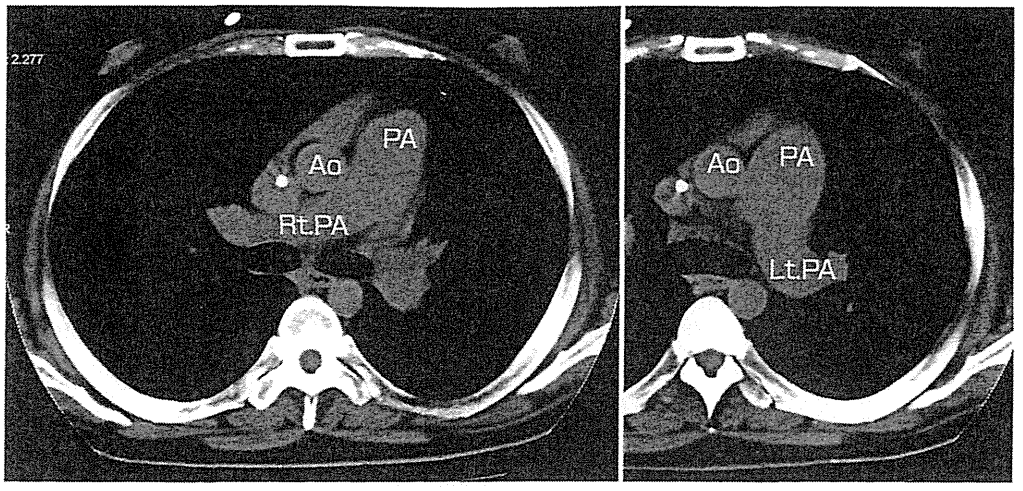


**図 3　PVOD 症例の単純 CT 像（縦隔条件）**
上行大動脈（Ao）と比較すると肺動脈主幹部（PA）～左右肺動脈（Rt. & Lt. PA）が著明に拡大していることがわかる。

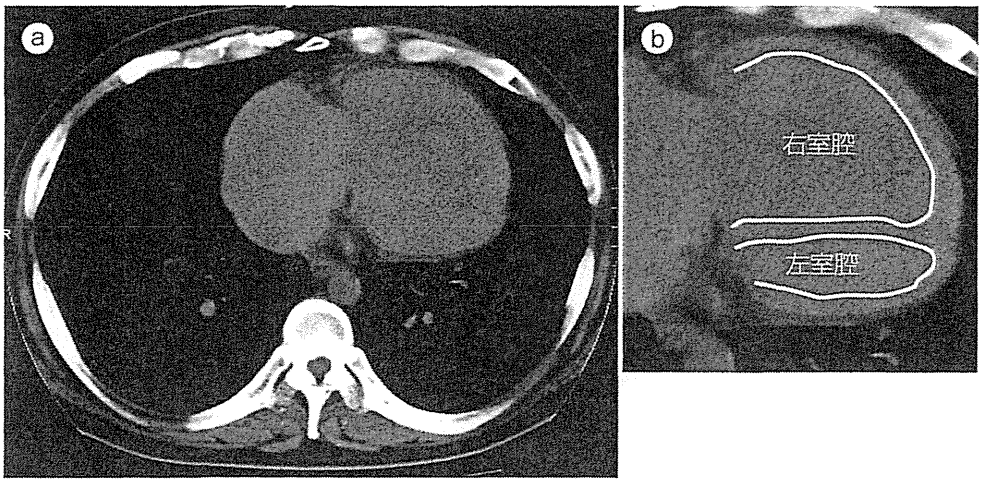


**図 4　PVOD 症例の単純 CT 像（縦隔条件）**
右心系の著明な拡大と心室中隔の左室側への圧排および左室の狭小化を認める。(b) に右室・左室内腔をトレースした拡大像を示す。

field of view（FOV）を用いて，高周波数関数により再構成を行った high-resolution CT（HRCT）では通常の CT よりも空間分解能に優れ，病理組織との対比も良好であることからより詳細な肺野病変評価が可能となっている。PVOD における HRCT 画像所見では小葉間隔壁の肥厚や小葉中心性の粒状影，背景にある血管や気管の構造を隠すことなく軽度の濃度の上昇がみられる「すりガラス様陰影（ground glass opacity）」などのいわゆる間質異常影が認められることがほかの肺高血圧起因疾患よりも頻度が高いと報告されている[1)~6)]。なお，それら所見の実際の頻度については，Resten らはすりガラス様陰影（辺縁は不明瞭で結節様）：73%，隔壁肥厚：93%，リンパ節腫大：80%，心嚢水：60%，胸水：27% などと報告している[3)]。また，日本人を対象にした報告でも上記同様に小葉間隔壁の

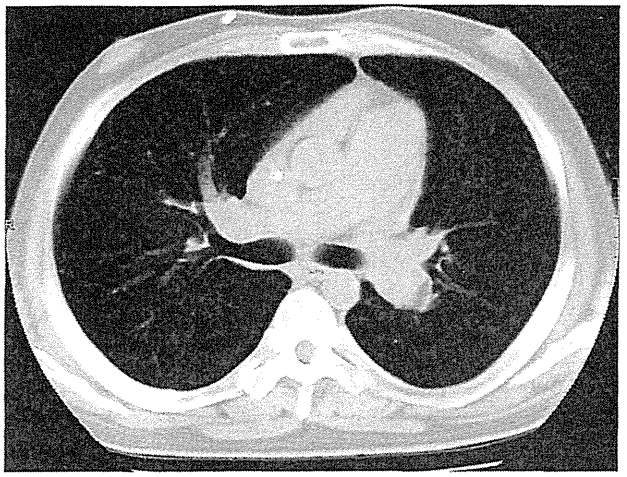

**図 5　PVOD 症例の単純 CT（肺野条件）**
全体的に肺血管影が目立つ。末梢には散在する粒状影や小葉中心性のすりガラス様陰影も認められる。

肥厚やすりガラス様陰影が多く見られると記されている[5)6)]。

図 5 に PVOD 症例の胸部単純 CT の肺野条件を示す。末梢に散在する粒状影や小葉中心性のすりガラス様陰影が認められる。さらに図 6 には同症例の HRCT を示すが，図 5 で示された所見よりさらに鮮明に小葉中心性に広がるすりガラス様陰影や小葉間隔壁の肥厚が観察される。

図 7 では別の PVOD 症例の HRCT を示す。図 5，6 で示した症例と比較してさらに鮮明な小葉中心性のすりガラス様陰影が認められる。

なお，これらの所見の頻度が高い理由としては肺静脈閉塞に伴う間質や肺胞の浮腫を反映していると考えられている[7)]。

一方，同じく肺高血圧症の起因疾患である IPAH では小葉中心性の粒状影・小結節影やすりガラス様陰影などは散見されるが小葉間隔壁の肥厚はあまり見られないとされており，両者を鑑別するうえでの相違点といわれる。実際に，IPAH と CT 所見を比較した報告によるとすりガラス様陰影は PVOD では症例の 87% で見られたものの IPAH では 33% しか見られず統計上も有意差（$p=0.03$）が認められ，その分布に関しても PVOD では小葉中心性の分布を示していた症例が IPAH よりも有意に多く認められたと記されている。さらに小葉間隔壁の肥厚は PVOD で 80%，IPAH で 0% とこれも有意差（$p<0.0001$）をもって PVOD に多く認められ，その一方で胸水は PVOD で多く認められる傾向にあったが IPAH との間に有意な差は見られなかったと報告されている[4)]。

図 8 に IPAH 症例の HRCT を示す。小葉中心性の非常に淡い粒状影を認めるが，先に提示した PVOD 症例のような小葉間隔壁の肥厚は見られず，またすりガラス様陰影も目立たない。

同じく肺高血圧症起因疾患として鑑別に挙げられる慢性血栓塞栓性肺高血圧症（chronic thromboembolic pulmonary hypertension：CTEPH）では，HRCT において比較的辺縁の明瞭な区域性のすりガラス様陰影，いわゆる「モザイクパターン」を認めることが多い[8)]のに対し，PVOD や IPAH では小葉中心性の淡い小結節影が認められることが多いことが肺野所見の一つの相違点とされている。また，CTEPH では造影 CT による肺動脈内の血栓付着が認められることが多いことが知られているが，末梢型 CTEPH と呼ばれる病態の中には CT での血栓の検出が困難な症例も認められ，造影所見のみではこれら疾患の鑑別が困難な場合も存在する。

図 9 に造影 CT では肺動脈内の血栓像を検出できなかった末梢型 CTEPH の HRCT を示す。HRCT では淡いすりガラス様陰影が目立

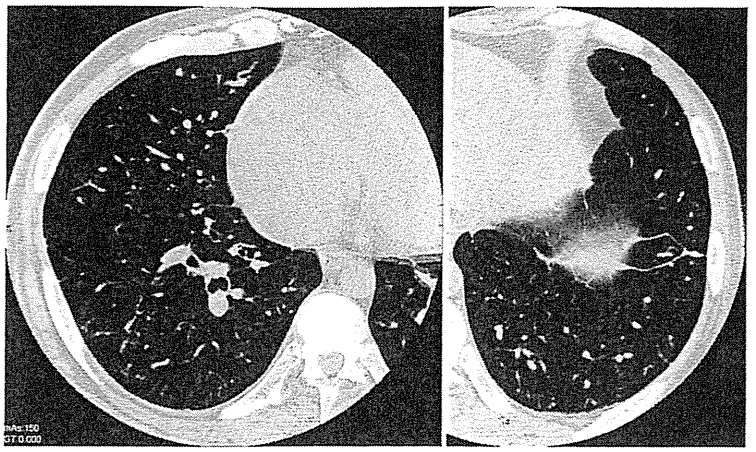

図 6　PVOD 症例の HRCT
小葉間隔壁の肥厚や小葉中心性の粒状影およびすりガラス様陰影の散在を認め，先の図 5 で示した通常 CT の肺野条件よりもその病変の分布や広がりが鮮明になっている。

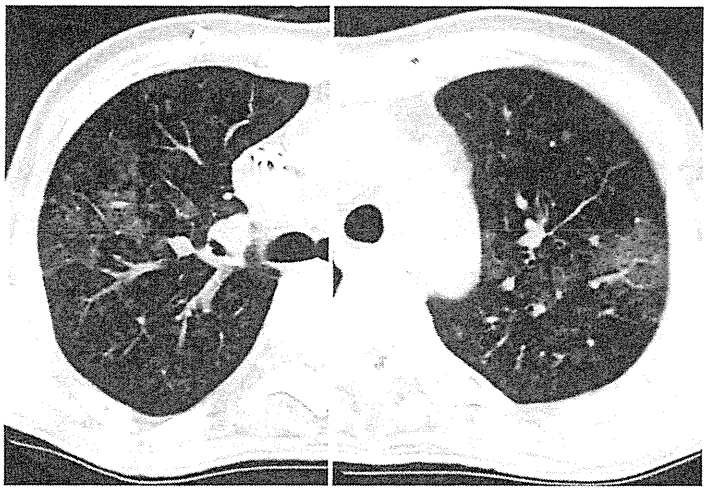

図 7　PVOD 症例の HRCT（図 5，6 と別症例）
先の症例と比較して，小葉中心性，汎小葉性に広がるすりガラス様陰影が明らかである。その他に小葉間隔壁の肥厚も認められる。

つが，PVOD 症例と異なり小葉中心性ではなく区域性のいわゆるモザイクパターンを示すことがわかる。

## 肺血流シンチグラフィー

肺血流シンチグラフィーで用いられる RI 薬剤「$^{99m}$Tc 標識大凝集性ヒトアルブミン（Macro aggregated human albumin：MAA）」は径が約 10～60 $\mu$m に調整された放射性微粒子薬剤で，静脈投与後肺毛細血管系よりサイズが大きいため毛細血管を通過することができずに補足され，微小塞栓となって肺に選択的に集積する。そこで画像化される肺内分布はその領域を流れる肺動脈血流量に比例することから画像診断に肺循環疾患の診断・鑑別

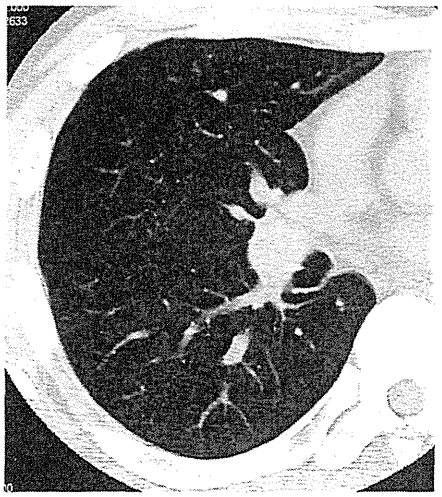

図 8 IPAH の HRCT
小葉中心性の淡い粒状影を認める。先に提示したPVOD症例と比較して，小葉間隔壁の肥厚は見られず，すりガラス様陰影も PVOD 症例ほど明らかでない。

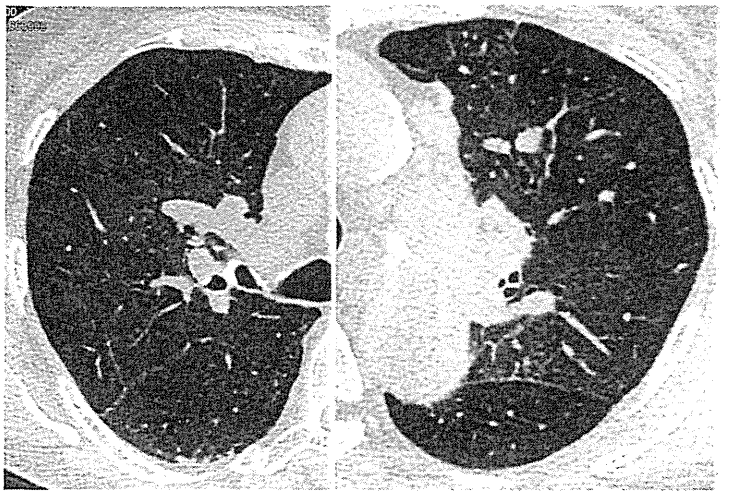

図 9 末梢型 CTEPH の HRCT
両肺に淡いすりガラス様陰影を認めるが，その分布は境界が比較的明瞭な区域性であり，モザイクパターンとも称される。PVOD のすりガラス様分布と異なることが窺える。

に多用されている。

この肺血流シンチグラフィーが診断上有用である肺高血圧症起因疾患としてはCTEPHが有名である。**図 10** にその肺血流シンチグラフィーを示すが，換気像は正常であるが血流像では両肺に外側域を中心に多発する楔状の血流欠損像を認め，いずれも換気像とミスマッチを呈している。

一方，同じく肺高血圧症起因疾患の IPAH 症例の肺血流シンチグラフィーを**図 11** に示す。IPAH では病期や罹病期間によりさまざまな肺血流所見を呈するといわれるが，典型的な所見としては**図 11** に示すような「mottled pattern」といわれる斑状の不均一血流所見が有名である。また，このような mottled pattern は IPAH のみならずシャント疾患に起因する肺高血圧症でも見られることが知られている。**図 12** にその画像を提示する。

それでは，PVOD の肺血流シンチグラフィー所見に関してはというと，小川らの報告では上葉有意の血流欠損像を認めるとされており[5]，この血流低下領域は換気像とミスマッチを呈するとの報告も見られる[9]。

そこで，当センターで剖検で確定診断に至った PVOD 5 症例に関して，その視覚評価を詳細に検討したところ，以下のような 3 系に分類できると思われた。

① 上肺野に限局する血流低下（2 例）：代表画像を**図 13** に示す。この血流分布パターンは既出の異常分布パターンと同様と思われる[5][9]。

② びまん性で細かい不均一肺血流分布（2 例）：代表画像を**図 14** に示す。読影所見として複数の放射線科読影医が「正常に近い血流分布であるが，完全には正常とはいえず，非常に細かい不均一性が見られる」と記述している。不均一な血流分布ではあるが，mottled pattern などのような粗大で強い不均一性ではなく，全体的に RI 集積が粗く見える細かな不均一性の印象がある。

③ CTEPH のような外側を中心に多発する楔状血流欠損（1 例）：代表画像を**図 15** に示

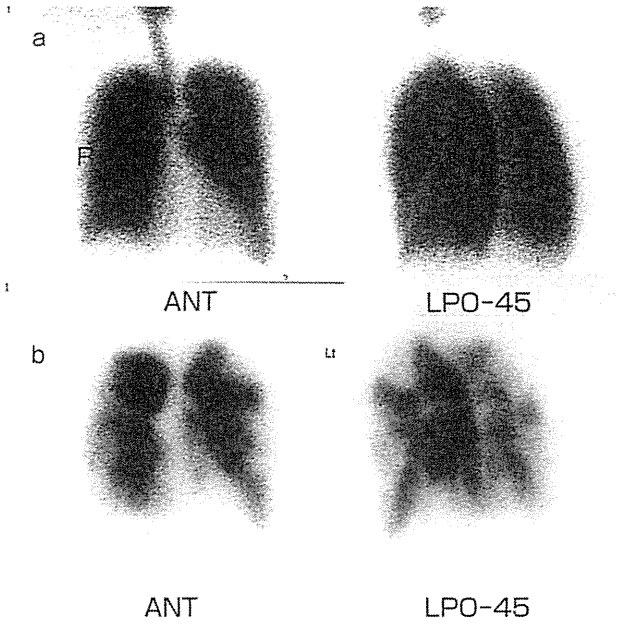


**図 10　CTEPH 症例**

a. 肺換気シンチグラフィー，b. 肺血流シンチグラフィー。

換気像（a）では異常を認めないが，血流像（b）では両肺ともに外側域を中心に多発する楔状血流低下～欠損領域を認め，換気像とのミスマッチを呈する。CTEPH の画像として典型的である。

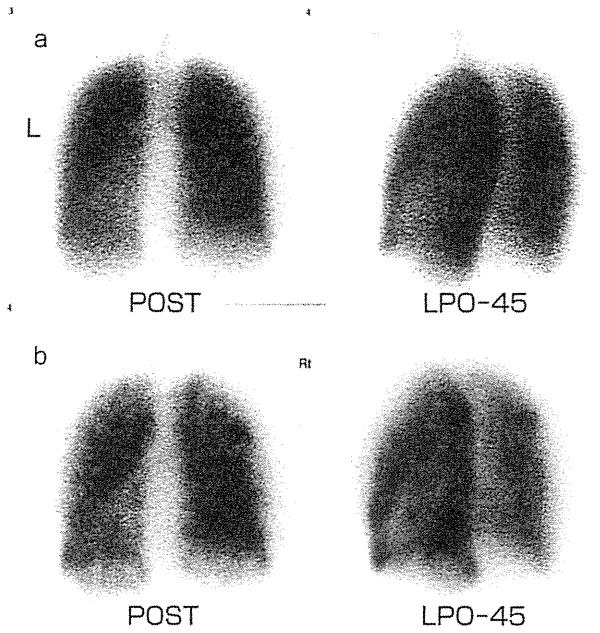


**図 11　IPAH 症例**

a. 肺換気シンチグラフィー，b. 肺血流シンチグラフィー。

換気像（a）では異常を認めないが，血流像（b）では両肺ともに全体的に不均一な血流を呈し，斑状影（mottled pattern）を認める。IPAH として矛盾しない画像所見であるが，このような mottled pattern は IPAH に特異的な所見ではない。

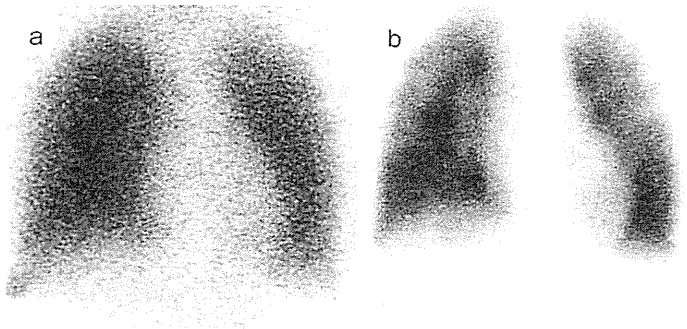


**図 12　シャント疾患による慢性肺高血圧**

心室中隔欠損症（VSD）で経過観察をされていた患者。徐々に肺高血圧が進行してきたため精査目的で入院。検査の結果，肺高血圧の原因は VSD 以外には認められなかった。平均肺動脈圧 PAP＝43 mmHg，Qp/Qs＝2.07。

換気像（a）では異常を認めないが，血流像（b）では両肺ともに全体的に不均一な血流を呈し，先の IPAH で見られたような斑状影（mottled pattern）を認める。Mottled pattern が IPAH に特異的な所見でないことが示唆される。

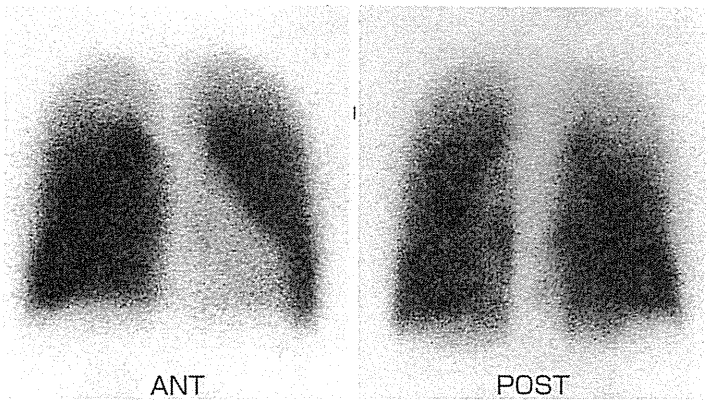


**図 13　PVOD 症例の肺血流シンチグラフィー**
上肺野に限局する血流低下パターン。全体的に非常に細かい不均一性を呈し，特に上肺野の血流は他領域と比較して低下している。

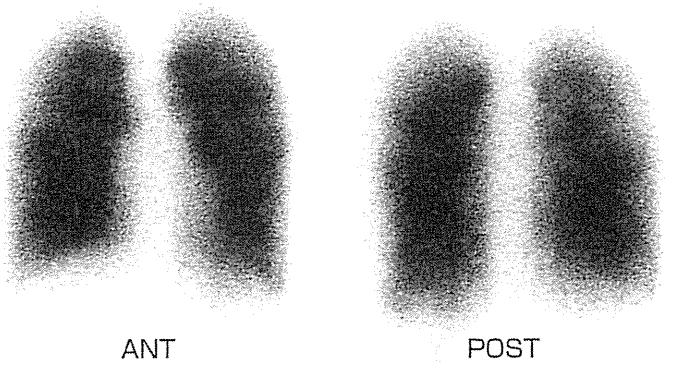


**図 14　PVOD 症例の肺血流シンチグラフィー**
びまん性で細かい不均一肺血流分布パターン。全体的に肺血流は不均一であるが，IPAH に見られる mottled pattern のような粗大な不均一性は認められない。

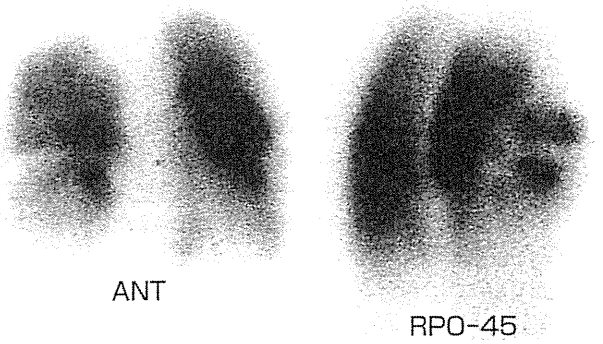


**図 15　PVOD 症例の肺血流シンチグラフィー**
多発する楔状血流欠損（CTEPH 様）パターン。外側域を中心に多発する楔状の血流低下～欠損を認め，CTEPH に典型的な血流異常パターン。なお，この症例は肺動脈造影検査においても肺動脈の多発狭窄～閉塞が認められており，肺動脈造影所見上も CTEPH として矛盾しない診断で，PVOD との鑑別は困難な症例であった。

す。なお，本症例は生前の肺動脈造影など他の画像所見上からCTEPHと診断されており，剖検で初めてPVODの確定に至った症例である。

以上の検討からはいずれにせよPVODでは血流の不均一性が一つの特徴所見として取り上げられる。ただし，これは視覚的・定性的評価であるため，鑑別診断への有用性を高めるためにこの不均一性を定量評価するべく，肺野に関心領域を設定し，関心領域内のカウント分布の標準偏差（カウントSD）を求め，正常例・IPAH症例・PVOD症例の3疾患群で比較するという追加検討を行った。具体的には①全肺野，②上・中・下肺野での比較，③外側域・内側域での比較の3点について検討を行ったが，いずれにおいても3疾患の間には有意な差を認めなかった。現段階では単なる肺血流カウント分布の不均一性を標準偏差などで計測するのみでは疾患鑑別には有用でないことが判明した。

分布の不均一性を定量化する方法として「フラクタル解析」が知られているが，過去には正常例・COPDおよび肺塞栓症の鑑別に肺血流シンチグラフィーの血流分布のフラクタル解析が有用であったとの報告もあり，今後はこのような新たな解析も検討に値すると思われる。

## おわりに

以上，PVODに関する画像診断の特徴や他疾患との鑑別点について過去の報告を含めて解説した。これまで述べてきたとおり，PVODに関して明らかに特異的な所見というものは乏しいことから，あくまで現段階ではこれらの所見からPVODを「疑うきっかけ」とすることが重要かと考えられる。本稿を参考にして，肺高血圧症症例に対して少しでもPVODの可能性について念頭に置いていただければ幸いである。


文献

1) Swensen SJ, Tashjian JH, Myers JL, et al. Pulmonary venoocclusive disease: CT findings in eight patients. AJR Am J Roentgenol 1996; 167: 937-40.
2) Almagro P, Julià J, Sanjaume M, et al. Pulmonary capillary hemangiomatosis associated with primary pulmonary hypertension: report of 2 new cases and review of 35 cases from the literature. Medicine 2002; 81: 417-24.
3) Resten A, Maitre S, Capron F, et al. Pulmonary hypertension: CT findings in pulmonary veno-occlusive disease. J Radiol 2003; 84: 1739-45.
4) Resten A, Maitre S, Humbert M, et al. Pulmonary hypertension: CT of the chest in pulmonary venoocclusive disease. AJR Am J Roentgenol 2004; 183: 65-70.
5) 小川愛子，松原広己．各種の肺高血圧症治療における診断のポイント．Pulmonary veno-occlusive diseaseとpulmonary capillary hemangiomatosisの診断のポイント．Ther Res 2012; 33: 1532-4.
6) 小川愛子，松原広己．疾患と検査値の推移．肺静脈閉塞症（pvod）．検と技2012; 40: 1435-9.
7) Grosse C, Grosse A. CT findings in diseases associated with pulmonary hypertension: a current review. Radiographics 2010; 30: 1753-77.
8) 井上征雄，谷本伸弘，佐藤　徹，ほか．肺高血圧症のCT所見：特に原発性肺高血圧症と慢性肺血栓塞栓症の鑑別を中心に．日呼吸会誌2006; 44: 485-91.
9) Bailey CL, Channick RN, Auger WR, et al. "High probability" perfusion lung scans in pulmonary venoocclusive disease. Am J Respir Crit Care Med 2000; 162: 1974-8.

ABSTRACT

## Characteristics of Imaging Findings in Patients with Pulmonary Veno-Occlusive Disease

Keisuke KISO*, Masahiro HIGASHI*

Pulmonary veno-occlusive disease (PVOD) is one of the rare diseases that cause pulmonary artery hypertension (PAH). Diagnosis of PVOD is confirmed by histopathological examination. However, early diagnosis with other medical tests is difficult, and many patients with PVOD have been diagnosed at autopsy. I discuss the relevant characteristics of PVOD that might be observed in images obtained using chest radiography, computed tomography (CT), and lung perfusion scintigraphy, and how these findings differ from other PAH diseases. In chest radiographs and conventional CT scans, cardiomegaly and pulmonary artery dilatation, which are reflections of right heart overload due to pulmonary hypertension, are often observed. Furthermore, in patients with PVOD, a high-resolution CT (HRCT) scan often reveals ground glass opacity with a centrilobular distribution and interlobular septal thickening, findings that are less frequently observed in cases of idiopathic PAH (IPAH) and chronic thromboembolic pulmonary hypertension (CTEPH). In lung perfusion scintigraphy scans, a general heterogeneity of count distribution and upper lobe hypoperfusion are frequently observed in cases of PVOD, but the degree of count distribution heterogeneity is less than that seen in patients with IPAH (e. g., mottled pattern). Although PVOD has few disease-specific characteristics that can be observed with imaging modalities, a consideration of the image findings mentioned above might facilitate early diagnosis of PVOD.

(Authors')

*Department of Radiology, National Cerebral and Cardiovascular Center, Suita*